PHYSICAL REVIEW D **96,** 076019 (2017)

Color screening in flux tubes and in the color Coulomb potential from QCD field correlators

M. S. Lukashov[1,2,*] and Yu. A. Simonov[1,†]

[1]*Alikhanov Institute for Theoretical and Experimental Physics, B. Cheremushkinskya 25, 117218 Moscow, Russia*

[2]*Moscow Institute of Physics and Technology, Institutskiy per. 9, 141700 Dolgoprudny, Moscow Region, Russia*

(Received 15 July 2017; published 30 October 2017; corrected 7 November 2018)

Colorelectric and colormagnetic structure of the flux tubes, connecting heavy quark and antiquark, is investigated in the framework of the field correlator method which describes all resulting fields in terms of correlators D^E and D_1^E. The latter have been computed via gluelumps, which allows us to predict the resulting distribution of color fields $\mathbf{E}(\mathbf{r})$, and colormagnetic currents $\mathbf{k}(\mathbf{r})$ in the flux tubes. It is shown, that at large distances $r \gg \lambda \approx 0.2$ fm the whole structure of fields and relations between them is similar to that of the dual superconductor theory, but the basic dynamics, including small distances, is given by field correlators of the real stochastic vacuum. The important contradiction between the strong screening of color fields in the width of flux tubes and almost no screening in the perturbative $Q\bar{Q}$ potential is resolved.

DOI: 10.1103/PhysRevD.96.076019

I. INTRODUCTION

The flux tubes between heavy quark and antiquark are considered as a necessary consequence of the color confinement mechanism, and were investigated numerically on the lattice during the last three decades, see, e.g., [1–24].

It was understood that this physical phenomenon should exist, whatever is the mechanism of color confinement, and hence only the detailed structure of flux tube fields can distinguish between different models of confinement.

One of the most popular, however not derived from QCD, is the model of dual superconductor (MDS) [25,26], where the QCD vacuum can be represented as a coherent state of colormagnetic monopoles. The numerous studies, both in theory and in numerical lattice works, have been done for the last two decades, trying to find the reasonable arguments and explicit formalism for MDS, see the review papers [27,28] and the references therein.

The difficulty of this approach is the lack of colormagnetic monopoles as real physical objects or Euclidean solutions of QCD, so that one should consider those as effective degrees of freedom in the real physical vacuum of QCD.

Meanwhile the quantitative theory of color confinement was suggested in [29–31] based on vacuum field correlators, developed in detail for application in hadron properties [32,33], including theory of Regge trajectories etc., the theory of chiral symmetry breaking [34], perturbation theory [35], and the QCD thermodynamics [36].

Field correlators can be found from the solution for the gluelump Green's functions of [37–39], which are connected back to field correlators in a self-consistent way [40–42], which allows us to define their properties for distances $r > \lambda$, where $\lambda \approx 0.2$ fm is the vacuum correlation length, $\lambda \sim 1/M_{\rm glp}$, $M_{\rm glp}$ is the lowest gluelump mass.

The problem of flux tubes in the framework of field correlator formalism was discussed in the review papers [43,44], where it was shown, that the basic properties of flux tubes are easily obtained from this formalism.

Recently a new formulation of the QCD equation of state and temperature transition was accomplished [45], which required a very detailed structure of the confinement dynamics, i.e., of the properties of field correlators, and those can be tested in the flux structure.

The latter, as shown below, define all the fields in the flux tube, and inversely, the study of flux tube fields gives information about details of field correlators, i.e., the details of the confinement mechanism.

From this point of view the flux tubes are an important source of information about the structure of confinement, including the temperature dependence of its constructing details.

Recently new lattice measurements of flux tube structure have been done in [46–48] and specifically in [46] the first accurate results have been obtained both for $SU(3)$ and $2+1$ QCD. It is the purpose of the present paper to compare these results with our analytic approach and to draw some conclusions on the mechanism of flux tubes and confinement.

The extended study of flux tubes in the framework of field correlator method (FCM) was done in [44], where the CE field distribution $\mathbf{E}(\mathbf{r})$ was found in terms of the confining correlator $D^E(x)$ and perturbative correlator $D_1^E(x)$, yielding the standard picture of the QCD string between two sources Q and $\bar{Q}$. In addition an important step was done, defining

*lukashov@phystech.edu
†simonov@itep.ru

the colormagnetic current $\mathbf{k}(\mathbf{r})$, which has the form of rings around the string, and it was also shown, that the "dual" London equation $rot\ \mathbf{k} = \lambda^{-2}\mathbf{E}(r)$—is satisfied at large distances from the string axis, $r \gg \lambda$.

This fact actually supports the idea, that the field correlator theory of confinement at large distances to some extent is equivalent to the dual superconductor picture, however the former allows to describe the flux tube fields at all distances.

It is one of the aims of our paper, to go further in this direction and in particular to present the distribution $|\mathbf{k}(\mathbf{r})|$ as a function of r, which can be further computed numerically on the lattice.

In addition, an interesting consequence of our theory is the distribution of the CE field $\mathbf{E}$, which is produced by the color charges and screened in the transverse, but not longitudinal direction as described by the correlator D_1^E and has no equivalent in MDS.

Indeed, the FC describe two kinds of CE fields, $E^{(1)}$ and $E^{(D)}$ due to correlators D^E and D_1^E respectively, and they have completely different distributions, in particular, D^E gives the main body of the flux tube,while D_1 gives the screening of the color Coulomb interaction.

Actually in [44], the important problem of the screening of perturbative fields due to confinement was not fully investigated, and instead there was a requirement of this screening at large distances, $r \gg \lambda$, where $\lambda \approx 0.2$ fm is the vacuum correlation length. Below we give the full answer to this problem of screening, based on the theory of confinement.

Another important development of the analysis of flux tube is its temperature variation, which was done on the lattice in [49]. This allows to measure the T dependence of correlators D^E, D_1^E, which plays the crucial role in the temperature transition region, as shown in [45].

The paper is organized as follows. In the next section we list the basic definitions and equations of the FCM, related to flux tubes, and in Sec. III we define the fields inside flux tubes in terms of FC, and magnetic currents. In Sec. IV our results are shown and compared to existing data for $T = 0$. Discussion of results and prospectives are given in the concluding section.

II. FIELD CORRELATORS IN QCD

The vacuum fields $F_{\mu\nu}(x)$ in QCD without external currents are necessarily stochastic and can be characterized by the set of field correlators (FC), which in the gauge invariant form for the lowest one, the Gaussian, [29–31] can be written as

$$\begin{aligned} g^2 D^{(2)}_{i4k4}(x-y) &\equiv \frac{g^2}{N_c}\langle \mathrm{tr}_f(F_{i4}(x)\Phi(x,y)F_{k4}(y)\Phi(y,x)\rangle \\ &= (\delta_{ik})D^E(x-y) + \frac{1}{2}\left(\frac{\partial}{\partial x_i}[h_k + \mathrm{perm}]\right)D_1^E(x-y), \\ h_\lambda &= x_\lambda - y_x. \end{aligned} \tag{1}$$

The temporal Wilson loop in terms of this basic FC can be written as [29–31] via colorelectric FC, D^E and D_1^E

$$\begin{aligned} W(C) &= \frac{1}{N_c}\left\langle \mathrm{tr}P\exp\left(ig\int_C dz_\mu A_\mu(z)\right)\right\rangle = \frac{1}{N_c}\left\langle \mathrm{tr}P\exp\left(ig\int_{S_{\min}} d\sigma_{\mu\nu}F_{\mu\nu}\right)\right\rangle \\ &= \frac{1}{N_c}\mathrm{tr}P\exp\left[-\frac{g^2}{2}\int d\sigma_{\mu\nu}d\sigma_{\lambda\rho}\langle F_{\mu\nu}F_{\lambda\rho}\rangle + \cdots\right] \cong \exp\left(-S_{\min}\frac{1}{2}\int D^E(z)d^2z\right), \end{aligned} \tag{2}$$

which implies that the string tension is expressed via $D^E(z)$ as

$$\sigma^E = \frac{1}{2}\int d^2z D^E(z). \tag{3}$$

In (3) the integration is over the minimal surface $S_{\min}$ inside the Wilson loop C.

Using D^E and D_1^E one can define the instantaneous interaction between fundamental or adjoint color changes, as it shown in the Appendix.

Note that $D^E(x)$, which enters in (2), generates the scalar potential $V_D(r)$

$$V_D(r) = 2c_a\int_0^r (r-\lambda)d\lambda\int_0^\infty d\nu D^E(\lambda,\nu) = V_D^{(\mathrm{lin})}(r) + V_D^{\mathrm{sat}}(r). \tag{4}$$

The FC D_1^E, which enters in the full derivative in (1), creates the vectorlike interaction

$$V_1(r) = c_a \int_0^r \lambda d\lambda \int_0^\infty d\nu D_1^E(\lambda,\nu), \qquad c_{\rm fund} = 1,$$
$$c_{\rm adj} = \frac{C_2({\rm adj})}{C_2(f)} = \frac{2N_c^2}{N_c^2-1}. \tag{5}$$

Equations (4) and (5) yield the information on correlators D^E, D_1^E, which can be obtained from the study of $Q\bar{Q}$ potentials $V_D(r), V_1(r)$. In what follows we shall exploit another way: on one side we shall define D^E and D_1^E via gluelump Green's function, on another side we find the structure of flux tubes with the help of D^E, D_1^E. In this way the data on flux tubes can be predicted and compared with lattice or experimental sources.

Until now the properties of D^E and D_1^E were not defined and to get information on that, one should exploit their connection to the gluelump Green's function, as it was done in [40–42]. Namely, $D^E(x)$ is expressed via the two-gluon-gluelump Green's function $G^{(2g)}(x,y)$

$$D^E(x-y) = \frac{g^4(N_c^2-1)}{2} G^{(2g)}(x,y) \approx g^4 N_c C_2(f) G^{(2g)}(x,y). \tag{6}$$

The lowest eigenvalues and the asymptotics of $G^{(2g)}$ were found in [37], namely $M_0^{(2gl)} \approx 2.5$ GeV, and from [40–42]

$$G^{(2g)}(x)(x \gg 1/M_0^{(2gl)}) \approx 0.108\sigma_f^2 e^{-M_0^{(2gl)}|x|}. \tag{7}$$

The insertion of (7), (6) into (4) immediately yields the potential $V_D^{(\rm lin)}(r)$ which is linear in whole region $r > 1/M_0^{(2g)} \approx 0.1$ fm. This fact agrees well with all experimental and numerical data.

It is interesting, that the same approach of two-gluon gluelump asymptotics for the colormagnetic function $D^H(x-y)$ yields [50] the well-known relation, found also on the lattice [51]

$$\sigma^H = g^4(N_c^2-1)T^2 c_\sigma, \qquad c_\sigma = {\rm const}. \tag{8}$$

In contrast to that, the FC D_1^E is expressed via the one-gluon gluelump Green's function with the nonperturbative part, behaving asymptotically as [40–42]

$$D_1^{E({\rm nonp})}(x) = \frac{2N_c\alpha_s}{x} M_0^{(1gl)} \sigma_f e^{-M_0^{(1gl)}|x|} \tag{9}$$

where $M_0^{(1gl)} \cong 1.5$ GeV [37–39], while the total form, containing the perturbative part as shown in Appendix B, is

$$D_1^{E({\rm pert})}(x) = \frac{2(N_c^2-1)\alpha_s K_2(mx)}{N_c \pi x^2} + O(\alpha_s^2). \tag{10}$$

As a result, the FC D_1^E produces the interaction $V_1^E(r)$

$$V_1^E(r) = -\frac{(N_c^2-1)\alpha_s e^{-mr}}{2N_c r} + O(\alpha_s^2), \quad \text{where}$$
$$m = O(1\ {\rm GeV}). \tag{11}$$

One should stress at this point, that one-gluon and two-gluon gluelumps enter separately in their mass measurements both on the lattice [38,39] and analytically [37], yielding different values (2.5 GeV in (7) and 1.5 GeV in (9) in both approaches. On the other hand, when computing the FC via gluelumps, as in [40–42], the mixing term appears ($D^{(1)}_{\mu\nu,\lambda\sigma}$ in [40–42]) which mixes up two contributions and brings in an averaged value $\bar{M}$ of the order of 1.0 GeV. The resulting mass m of the order of $\bar{M}$ in Eq. (11) is the gluon screening mass.

At this point we turn to the measurements the flux tube fields, as it is done on the lattice, where one computes the average value of the contour, shown in Fig. 1, consisting of a small plaquette at the point x, connected by two fundamental lines to the Wilson loop of heavy quarks Q, $\bar{Q}$.

Here appears a new phenomenon, which might be called "the quenching of the screening gluon mass", namely, as shown in Fig. 2, the value of the one-gluon screening mass $M \cong 1.5$ GeV is obtained, when the parallel transporter in the transverse position is fixed, as shown in Fig. 1, where the double fundamental line in the transverse direction defines the form of the confining film in the gluelump Green's function.

On the other hand, measuring gluon exchange in the horizontal plane without any transporters, which limit the size of the confining film, one obtains, that the resulting minimal surface is a slightly deformed plane inside the big contour, as shown in Fig. 3. The energy of deformation is equal to $\varepsilon_{\rm plane} = \sigma \Delta S_{\rm min} = \sigma \frac{h^2}{L}$, where h is the average deflection of gluon path from the plane and L is plane length. This should be compared with the energy in the gluelump

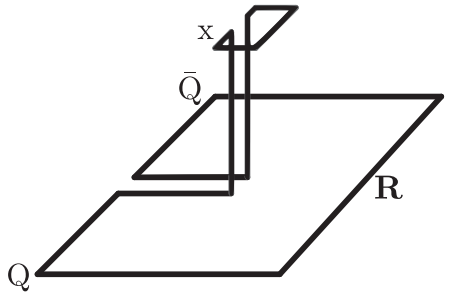

FIG. 1. The connected probe plaquette at the point x above the $Q\bar{Q}$ Wilson loop.

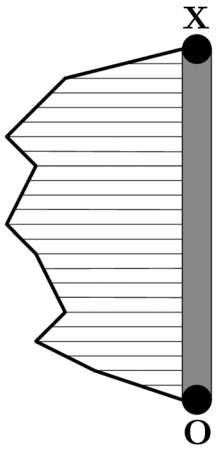

FIG. 2. The 1g gluelump configuration for the transverse probe.

case, $\varepsilon_{\rm glp} \cong \sigma h$, with the result $\varepsilon_{\rm plane} \ll \varepsilon_{\rm glp}$, meaning a strong damping of the Coulomb screening $M_{\rm scr}^{\rm Coul} \ll M_{\rm glp}$.

Moreover, the length L between consecutive gluon exchanges can be estimated from the action exponent $\exp(-V_{\rm Coul}(R)L)$, as $L^{-1} \sim V_{\rm Coul}(R) \sim \frac{4}{3}\frac{\alpha_s}{R}$ $(N_c = 3)$, leading to the result $\varepsilon_{\rm plane} = \sigma\frac{h^2}{L} \sim \frac{4}{3}\sigma\frac{h^2}{R}\alpha_s$. Thus the screening is additionally damped at large R, for the analytic treatment of this type of interaction (but without α_s/R) see [52].

It is clear from the analysis of [52], that the screening mass, corresponding to the Fig. 3, is the mass excitation of the static hybrid of the length L with the transverse excitation of the order of $\sqrt{12}/L$ and longitudinal $(\sigma/L)^{1/3}$. Defining L as before from the condition $\Delta t V_{\rm Coul} = O(1)$, one obtains for $R = 1$ fm for both excitations $\Delta m \approx 0.4$ GeV instead of 1.4 GeV for the one-gluon gluelump mass. Note also, that for the single gluon exchange, when Δt tends to infifnity, the screening mass Δm tends to zero.

Numerically on the lattice the static $Q\bar{Q}$ potential demonstrates [53,54] the linear plus pure Coulomb form. Our discussion above might give an answer to the similar point, raised recently in [55].

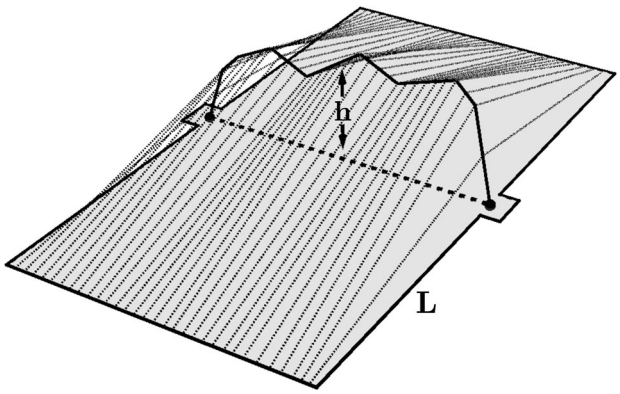

FIG. 3. The minimal area surface for the gluon exchange interaction.

In our case, where a part of parallel transporters is in the transverse direction, as in Fig. 1, one expects, that our mass m satisfies $M_{\rm scr}^{\rm Coul} < m < M_{\rm glp}$, and we choose explicitly in what follows for transverse $r_\perp$ distributions, $m = 1$ GeV, which we shall use to define the vacuum correlation length λ,

$$\lambda = \frac{1}{m} = 0.2 \text{ fm}. \tag{12}$$

To complete the picture of potentials V_D and V_1 one should mention another important feature of resulting potentials in (4), (11): as it is shown in the Appendix of [45], the terms $V_D^{\rm sat}(r)$ in (4) and $V_1^{(np)}(r)$ have different signs and almost fully compensate each other for low temperatures. As a result the interaction between two static charges acquires the well established form, confirmed on the lattice and in experiment:

$$V_{Q\bar{Q}}(r) = V_1^{(\rm pert)}(r) + V_D^{(\rm lin)}(r). \tag{13}$$

As we shall see below, this cancellation holds only for potentials, which are in-plane integrals of the FC, as in (4), (5). However, for the flux tube probes, which are mostly the out-of-plane integrals of FC, this full cancellation does not take place, and one has a possibility of defining the FC through the measurements of flux tube probes, which is especially interesting for nonzero T, and around $T = T_c$ [56–58].

In the next section we define the connected flux tube probes via field correlators, following [43,44] and adding a new contribution from the correlation $D_1^{(np)}$.

III. FLUX TUBE FIELDS VIA FIELD CORRELATORS

To measure field distributions around the static color charges Q, $\bar{Q}$, one can use the connected probe, defined by the contour C, shown in Fig. 1, as it is done on the lattice [1–24], and calculated in the FCM, see e.g. [43,44].

As shown in [44], Eq. (30), the resulting effective field $F_{\mu\nu}(x)$ is expressed via the FC, Eq. (1),

$$F_{\mu\nu}(x) = \int_S d\sigma_{\alpha\beta}(y) g^2 D^{(2)}_{\alpha\beta\mu\nu}(x-y). \tag{14}$$

Inserting (1) in (14) one obtains as in [44] the expression for the colorelectric probe $\mathbf{E}_i(\mathbf{r},\mathbf{R})$

$$E_i(\mathbf{r},\mathbf{R}) = n_k \int_0^R dl \int_{-\infty}^{\infty} dt \left(\delta_{ik} D^E(z) + \frac{1}{2}\frac{\partial(z_i D_1^E(z))}{\partial z_k}\right), \tag{15}$$

where $z = (\mathbf{r} - \mathbf{n}l, t)$, and $\mathbf{n} = \frac{\mathbf{R}}{R}$ is along the axis x_3, where the charges Q, $\bar{Q}$ are placed at the distance R, see Fig. 1.

Inserting the perturbative part $D_1^{E(\mathrm{pert})}$ from (10), one obtains the screened color Coulomb field

$$\mathbf{E}^{(1)}(\mathbf{r}) = \frac{(N_c^2-1)}{2N_c}\left(\frac{\alpha_s \mathbf{r}\chi(mr)}{r^3} - \frac{\alpha_s(\mathbf{r}-\mathbf{R})}{(\mathbf{r}-\mathbf{R})^3}\chi(m|\mathbf{r}-\mathbf{R}|)\right), \tag{16}$$

where the screening factor is $\chi(z) = (1+z)e^{-z}$, and at the midpoint between the charges one has

$$\mathbf{E}^{(1)}\left(\frac{\mathbf{R}}{2}\right) = \frac{4(N_c^2-1)}{N_c}\frac{\alpha_s \mathbf{R}}{R^3}\chi\left(\frac{mR}{2}\right). \tag{17}$$

Equation (17) contains both the standard perturbative part $E^{(1)} \sim \frac{\alpha_s}{R^2}$, at $R \ll \frac{1}{m}$ and the nonperturbative screening $E^{(1)} \sim \frac{\alpha_s m}{R} e^{-mR}$ at $R \gg \frac{1}{m}$. For the field correlators, as in (14), the mass, $m \approx 1$ GeV, while the screening in the one gluon exchange potential $V_1(r)$ Eq. (11), is much softer, as discussed in [59], see also Appendix B.

From (17) one can estimate $E_3^{(1)}$ at $R = 0.2$ fm, $m = 1$ GeV and $r_\perp = 0$. $E_3^{(1)}(0.5\text{ fm}, 0) = 0.122\alpha_s\ \mathrm{GeV}^2 \approx 0.05\ \mathrm{GeV}^2$ for $\alpha_s \cong 0.4$. In a similar way, using the asymptotics (7), and the relation (3), one has

$$D(z) = \frac{\sigma}{\pi\lambda^2}\exp\left(-\frac{|z|}{\lambda}\right), \qquad \lambda^{-1} \cong 1\ \mathrm{GeV}, \tag{18}$$

which yields for the colorelectric probe, following (15)

$$\mathbf{E}^D = \mathbf{n}\frac{2\sigma}{\pi}\int_0^{R/\lambda} dl \left|l\mathbf{n} - \frac{\mathbf{r}}{\lambda}\right| K_1\left(|l\mathbf{n} - \frac{\mathbf{r}}{\lambda}|\right). \tag{19}$$

For $R \to \infty$ one obtains from (19) the saturated colorelectric field at the distance $r_\perp$ from the axis

$$E_3^D(\mathbf{r}_\perp) = 2\sigma\left(1 + \frac{r_\perp}{\lambda}\right)\exp\left(-\frac{r_\perp}{\lambda}\right) \tag{20}$$

and the saturated on-axis value $E_3^{\mathrm{sat}}(\mathrm{on\ axis}) = 2\sigma$.

Summing up the contributions of (17), (19) for the field E_3 at the midpoint on the axis ($r_\perp = 0$), one has ($N_c = 3$)

$$E_3^{\mathrm{tot}}\left(\frac{R}{2}, r_\perp = 0\right) = \frac{32\alpha_s}{3R^2}\chi\left(\frac{mR}{2}\right) + \frac{2\sigma}{\pi}\int_0^{R/\lambda} dx \cdot xK_1(x). \tag{21}$$

Another interesting characteristics of flux tabes is the E_3 dependence on the distance to the $Q\bar{Q}$ axis, i.e., on $r_\perp$. Using (16), (19) one can write

$$E_3(r_\perp) \equiv E_3\left(r_\perp, \frac{R}{2}\right) = E_3^D\left(r_\perp, \frac{R}{2}\right) + E_3^{(1)}\left(r_\perp, \frac{R}{2}\right), \tag{22}$$

where

$$E_3^D\left(r_\perp, \frac{R}{2}\right) = \frac{2\sigma}{\pi}\int_{-\frac{R}{2\lambda}}^{\frac{R}{2\lambda}} dx \sqrt{x^2 + \frac{r_\perp^2}{\lambda^2}} K_1\left(\sqrt{x^2 + \frac{r_\perp^2}{\lambda^2}}\right), \tag{23}$$

$E_3^{(1)}$ is given in (16),

$$E_3^{(1)}\left(r_\perp, \frac{R}{2}\right) = \frac{4}{3}\alpha_s \frac{R\chi(m\sqrt{r_\perp^2 + \frac{R^2}{4}})}{(r_\perp^2 + \frac{R^2}{4})^{3/2}}. \tag{24}$$

In the next section we compare our results for $E_3(r_\perp)$ and $E_3^{\mathrm{tot}}(\frac{R}{2})$ with the lattice data [46].

We now turn to the effective magnetic monopole picture, which can be derived from our method, to compare it with the dual superconductor model.

To this end we as in [44] define first of all the magnetic current $\mathbf{k}$,

$$\mathbf{k} = \mathrm{rot}\mathbf{E}(\mathbf{r}, \mathbf{R}) = \mathrm{rot}(\mathbf{E}^D(\mathbf{r}) + \mathbf{E}^{(1)}(\mathbf{r})) \equiv \mathbf{k}_D + \mathbf{k}^{(1)}, \tag{25}$$

One can deduce from (16), that $\mathbf{E}^{(1)}$ at $r_3 = \frac{R}{2}$ (at the midpoint) does not have component along axis 1 and 2, so that it can be written as $\mathbf{E}^{(1)}(r_3 = \frac{R}{2}, r_\perp) = \mathbf{n}f^{(1)}(r_\perp^2)$, and hence $f^{(1)}(r_\perp^2) = E_3^{(1)}(r_\perp, \frac{R}{2})$ given in (22).

The same is true for E^D, Eq. (19), so that the total $\mathbf{k} = \mathbf{k}^{(1)} + \mathbf{k}_D$ is perpendicular to $\mathbf{n}$, as shown in Fig. 4.

Therefore $k_z = 0$, and $k_x = 2yf', k_y = -2xf'$ so that $\mathbf{kr} = 0$, which means, that vectors $\mathbf{k}$ form circular loops

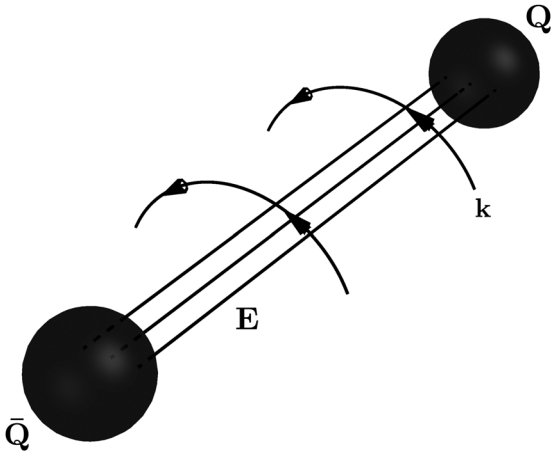

FIG. 4. Colormagnetic current k around the flux tube.

around the $(Q,\bar{Q})$ axis. The function $f^{(1)}(r_\perp^2)=E_3^{(1)}$ is given in (24), and one can calculate the $r_\perp$ dependence $|\mathbf{k}_\perp^{(1)}(r_\perp)|^2=(k_x^{(1)}(r_\perp))^2+(k_y^{(2)}(r_\perp))^2$,

$$(\mathbf{k}^{(1)}(r_\perp))^2=4r_\perp^2\left(\frac{\partial E_3^{(1)}}{\partial r_\perp^2}\right)^2. \tag{26}$$

The function $\mathbf{k}_D(r_\perp)$ is obtained from (23), where one can use the relation $\frac{d}{dz}(zK_1(z))=-zK_0(z)$, with the result

$$\mathbf{k}_D^2(r_\perp)=\frac{4\sigma^2r^2}{\pi^2\lambda^4}\left(\int_{-\frac{R}{2\lambda}}^{\frac{R}{2\lambda}}dxK_0\left(\sqrt{x^2+\frac{r_\perp^2}{\lambda^2}}\right)\right)^2 \tag{27}$$

In the case when $\mathbf{k}_D$ and $\mathbf{k}^{(1)}$ can be both nonzero, the resulting $\mathbf{k}(r_\perp)$ is

$$\begin{aligned}\mathbf{k}(r_\perp)&=\mathbf{k}^{(1)}+\mathbf{k}_D\\&=-(\mathbf{n})_\varphi r_\perp\left(\frac{2\sigma}{\pi\lambda^2}\int_{-\frac{R}{2\lambda}}^{\frac{R}{2\lambda}}dxK_0\left(\sqrt{x^2+\frac{r_\perp^2}{\lambda^2}}\right)+\frac{\partial f^{(1)}}{\partial r_\perp^2}\right)\end{aligned} \tag{28}$$

and $\mathbf{n}_\varphi\mathbf{r}_\perp=0,\mathbf{n}_\varphi^2=1$.

The most important point for the connection to the superconducting model is the dual London equation $\mathrm{rot}\mathbf{k}=\lambda^{-2}\mathbf{E}$, which, as shown in [44], is supported asymptotically $(r_\perp\to\infty)$ by the relation for the saturated string $(R\to\infty)$

$$\begin{aligned}\mathrm{rot}\mathbf{k}_D&=\gamma_D(r_\perp)\lambda^{-2}\mathbf{E}^{(D)}(r_\perp),\\\gamma_D(r_\perp)&=\frac{r_\perp/\lambda-2}{r_\perp/\lambda+1},\qquad\gamma(\infty)=1.\end{aligned} \tag{29}$$

IV. FIELD CORRELATORS VS DUAL SUPERCONDUCTOR MODEL

At this point it is interesting to compare the FCM and MDS approaches, their results and interpretation.

In the MDS the basic Lagrangian refers to the 4d version of the Ginzburg-Landau, or the Abrikosov-Nielsen Olesen (the Abelian Higgs) model

$$L=-\frac{1}{4}F_{\mu\nu}^2-|D_\mu\varphi|^2-\frac{\lambda}{4}(|\varphi|^2-\varphi_0^2), \tag{30}$$

where the Higgs field φ provides the mass of the electric field, $m^2=\delta^{-2}=2e^2\phi_0^2$, while the Higgs mass $m_\phi^2=2\lambda\phi_0^2$ defines the correlation length ξ. For the standard type II superconductor one has $\delta\gg\xi$.

It is argued, that in general the flux tubes can occur for a wide region of δ, ξ values, including the type I case, $\delta\lesssim\xi$.

In the DSM interpretation of the lattice data one uses λ,φ_0 as fitting parameters and it was found in [46], that they correspond to the type I superconductor. There are three main properties in the MDS approach, which need clarification:

(1) The typical consequence of (30) is the exponential screening of the electric field at large transverse distances $r_\perp$ in agreement with London equations, as we discussed above, but also a logarithmic divergence at small $r_\perp$, which is not seen numerically on the lattice. To avoid this divergence the authors of [46] exploit an approximate variational solution from [60], containing extra parameters.

(2) It is argued in [61], that at the large distances between charges the physical picture of flux tubes corresponds to the effective string theory of the Nambu-Goto type, rather than to the DSM.

(3) In general the Lagrangian (30) contains scalar massive fields as extra degrees of freedom, which should display themselves in some way, especially for $\delta\sim\xi$, and which are not seen in QCD and in numerical lattice data. In contrast to that, the FCM does not contain any extra parameters, and defines all parameters in term of string tension σ, which can be observed and computed numerically. In terms of σ can be expressed also of all the gluelump masses, defining the screening of flux tubes at the scale of 0.2 fm.

(4) One of the most important predictions of FCM for the flux tubes is the asymptotic value of the on-axis field $E_3(R)$ at large R equal to 2σ, which is well supported by lattice data [46]. On the MDS side unfortunately there are no explicit predictions, and the values given by the MDS variational equation of the type of Ref. [60], depend on extra parameters.

(5) Practically very important is the existence of the color Coulomb interaction, which is superimposed on the scalar confinement,with almost no screening at large distances, as discussed above and well known in experiment and on the lattice. One should stress at this point, that the main properties of the confinement follow from the Wilson loop structure of the $Q\bar{Q}$ interaction, with the surface of minimal area, which implies, that an additional adjoint line of color Coulomb interaction should belong to this surface. This fact strongly suppressed the fluctuation of the gluon trajectory and as a result also the gluon screening mass, as we have discussed in Sec. II.

It is not clear how one can describe the scalar confinement and the vector color Coulomb interaction simultaneously in the framework of the MDS or any theory of the Abelian Higgs type.

(6) As a final point of our comparison, we discuss the Lorentz properties of the confining interaction. Indeed, there exists a strong limitation on the vector admixture in the confining interaction. As shown

in [62,63], the spectrum of the Dirac equation with the dominating confining vector part does not contain bound states. This feature is connected to the Klein paradox with multiple $q\bar{q}$ pair production. On the physical side the observed experimentally negative spin-orbit term in the $q\bar{q}$ interaction is due to scalar confinement, thus supporting its scalar nature.

Now it is important, that in the FCM one generates confinement with scalar properties, as it was shown in [63,64] and also in connection with chiral symmetry breaking, in [65]. The same result one obtains using MDS, if one finds the correspondence between field correlators in MDS and FCM, as it was done in [59]. Thus summarizing, one can conclude, that in the MDS one is able to construct reasonable approximate solutions of the Lagrangian of Abrikosov-Nielsen-Olesen type, which can be similar to the FCM scalar confinement flux tubes, but this correspondence at present does not cover all details and types of interaction.

V. RESULTS AND DISCUSSION

To compare with recent accurate lattice data [46], we are using the data, shown in Fig. 4 of this paper for two types of behavior: first, we are using the data [46] for $E_3^{\rm tot}(R)$ here $R = 0.76$ fm, 0.95 fm, 1.14 fm, 1.33 fm and calculate our E_3 from Eq. (21) for these values of R. The results are shown in Fig. 5 with $\alpha_s = 0.4$, $m = 1$ GeV, $\sigma = 0.18$ GeV^2. One can see a reasonable agreement of our theory with the data,where a slow decrease of $E_3^{\rm tot}(R)$ is due to $E_3^{(1)}$, while the saturation at $E_3 = 2\sigma$ is due to E_3^D.

To check the $r_\perp$ dependence, we again are using data of [46] and present our results for the quoted values of R in Figs. 6–9. One can see again a reasonable agreement at the level of $O(5\%)$ for $r_\perp < 0.5$ fm. Note, that our parameters α_s, m, σ are fixed at the physically relevant values, $\alpha_s(Q \sim 1\ \text{GeV}) = 0.4$, $\sigma = 0.18$ GeV^2.

Finally, in Fig. 10 we demonstrate the $r_\perp$ dependence of the modulus of $|\mathbf{k}(r_\perp)|$, given by Eqs. (26), (28). One can see the exponential decay at large $r_\perp$, typical for the color screening of massive gluon fields.

At this point one can compare our results with the MDS picture. In general, one can treat the dual Abelian Higgs picture and different versions of MDS in the same language as in FC, calculating D^E, D_1^E via solutions of Ginzburg-Landau equations etc.

This type of analysis was done in [59], where D^E, D_1^E have been related with the dual filed propagator in the Abelian Higgs model. However, parameters of the model and the form of D, D_1 are not fixed, e.g the connection of sigma and the mass $m = 1/\lambda$, whereas in the FC approach in QCD the product $\sigma\lambda^2$ is fixed by the gluelump mechanism and ensures Casimir scaling, observed on the lattice. Summarizing, in the FC approach all observables are

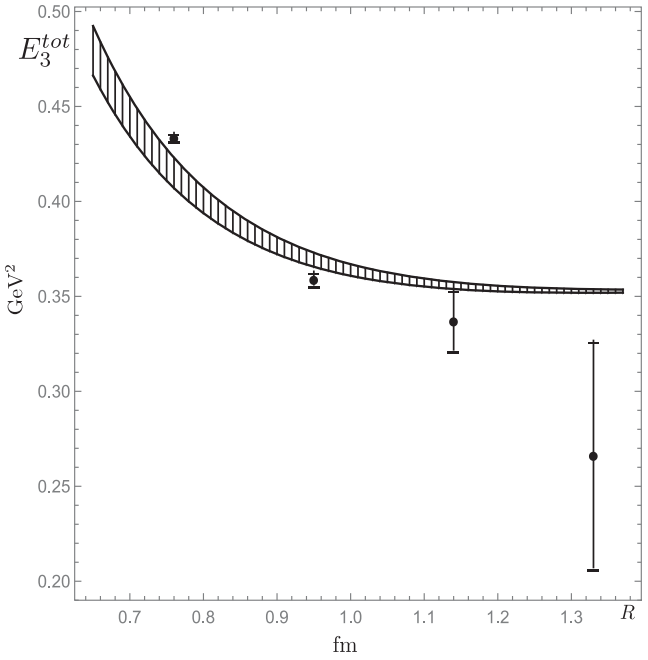

FIG. 5. $E_3^{\rm tot} = E_3^{\rm tot}(\frac{R}{2}, r_\perp = 0)$. The tube length dependence of the CE field strength at the midpoint. The shaded region corresponds to $\alpha_s = 0.4$ (lower curve) and $\alpha_s = 0.45$ (upper curve). The points with error bars are from the lattice measurements in [46].

defined by the only nonperturbative scale (in addition to quark masses), which can be chosen as σ.

In [46] the theoretical form of $E_3(r_\perp)$ was chosen, according to the solutions of the Ginzburg-Landau

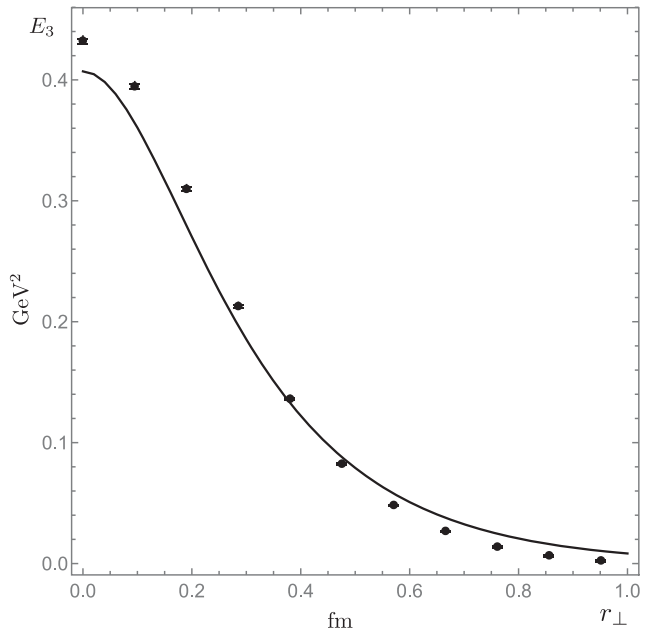

FIG. 6. $E_3 = E_3(r_\perp, R = 0.76\ \text{fm})$. The transverse radius dependence of the CE field strength for the fixed flux tube length $R = 0.76$ fm. The dots with error bars are from the lattice measurements in [46].

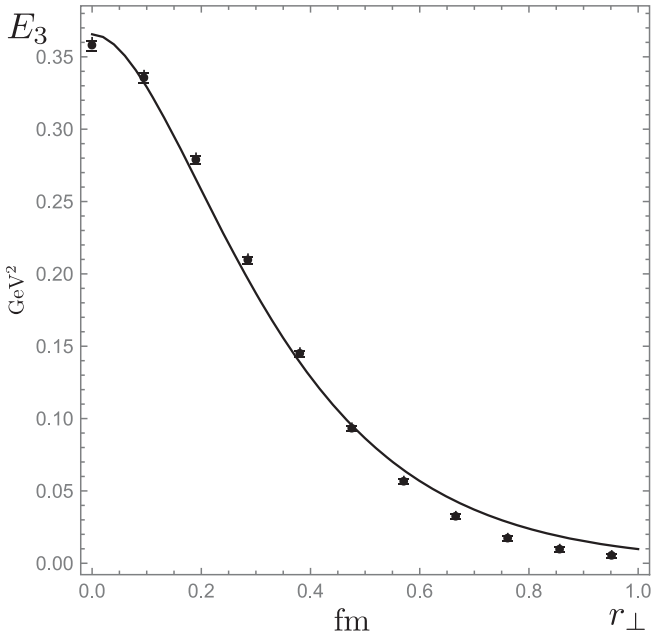

FIG. 7. $E_3 = E_3(r_\perp, R = 0.95\ \text{fm})$. The transverse radius dependence of the CE field strength for the fixed flux tube length $R = 0.95$ fm. The dots with error bars are from the lattice measurements in [46].

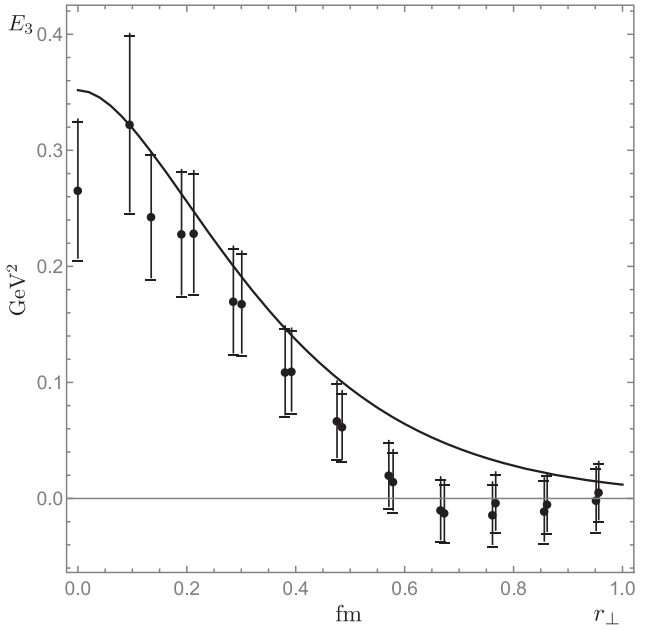

FIG. 9. $E_3 = E_3(r_\perp, R = 1.33\ \text{fm})$. The transverse radius dependence of the CE field strength for the fixed flux tube length $R = 1.33$ fm. The dots with error bars are from the lattice measurements in [46].

equations, suggested in [60], with parameters, ensuring a good agreement with the lattice data. These parameters correspond to the superconductor of the first order, where the coherence length ξ is larger, than the penetration length λ. However, the three flux tube parameters depend (moderately) on the length of the flux tube R.

Summarizing,we have derived two components of the CE fields in the flux tube and have shown the strong transverse screening of CE fields on the length $\lambda = 0.2$ fm. We also found the slight decrease and saturation of the on-axis field $E_3(R)$ at large R. We have found a reasonably

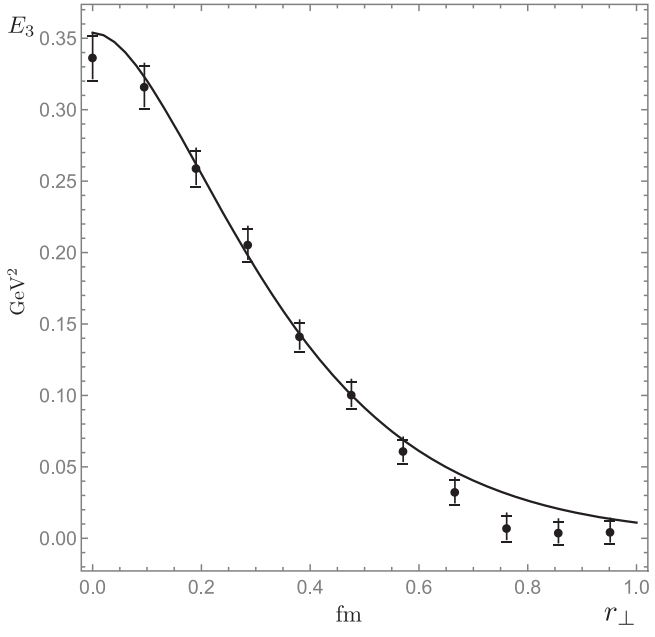

FIG. 8. $E_3 = E_3(r_\perp, R = 1.14\ \text{fm})$. The transverse radius dependence of the CE field strength for the fixed flux tube length $R = 1.14$ fm. The dots with error bars are from the lattice measurements in [46].

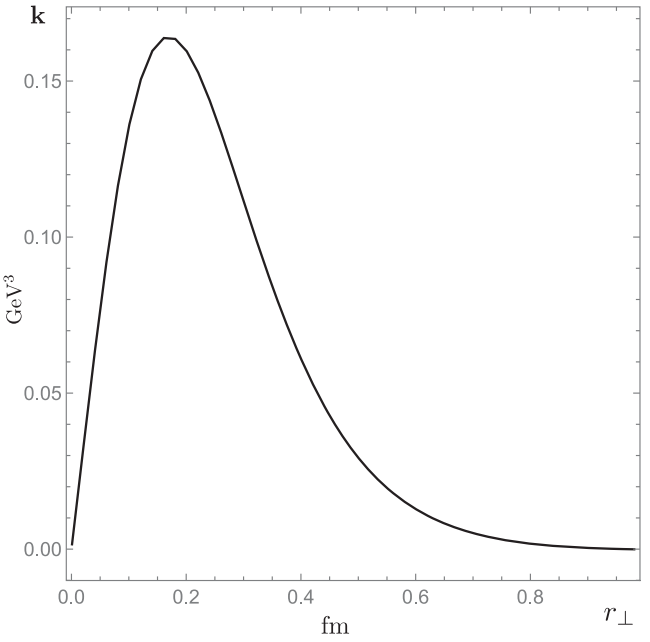

FIG. 10. The transverse radius dependence of the CM current $|\mathbf{k}(r_\perp)|$ at $R = 0.76$ fm.

good agreement of our results with the latest lattice data of [46], confirming the applicability of our theory using standard parameters, independent of R.

Finally, we have presented arguments, why the in-plane screening of the gluon exchange (color Coulomb interaction) is strongly damped, as compared with the transverse screening of the same interaction.

In the previous section we have compared our approach with the MDS model in the interpretation of the lattice results. We have argued, that in the MDS there is still no strictly defined formalism with fixed parameters, which is able to reproduce the whole set of phenomena, including both confinement and gluon exchanges, which is the basics of strong interaction in QCD, while it is well described by the FCM.

To extend our discussion of possible applications of the FCM and MDS, we refer to the interesting results in [66], concerning the flux tubes in the $(q\bar{q}g)$ (hybrid) system. In this case the object was a system of static quark-adjoint charge-antiquark system of variable forms, which included convolution of $q\bar{q}$, transforming two adjacent fundamental strings into one adjoint string. This configuration corresponds to two fundamental Wilson loops having one side in common with varying sizes and angle between surfaces. This problem is actually the problem of two interacting Wilson loops, and the general formalism for its solution was given in [67]. The extension of the results of [67] to the case of static hybrid, considered in [66], can be done in the same formalism and would be of great interest.

Finally we mention another interesting possible development of the FCM formalism in treating arbitrary gauge groups instead of $\mathrm{SU}(N_c)$, considered above—for a review and references see [68–70]. It is clear, that the main result of [65], establishing the Casimir scaling of the string tension for the group G_2, is well reproduced in the FCM, provided the Gaussian approximation (keeping only quadratic terms $\langle FF\rangle$) holds.

Indeed, the confinement is best illustrated by the Wilson loop form for any group, where neglecting higher order $O(\langle FFFF\rangle)$ terms one can write

$$\langle W(C)\rangle = \left\langle \exp\left(ig\int_C A_\mu dz_\mu \right)\right\rangle = \left\langle \exp\left(ig\int_S F_{\mu\nu}(u)d\sigma_{\mu\nu}\right)\right\rangle$$
$$\cong \exp\left(-\left\langle \int g\hat{F}_{\mu\nu}(u)d\sigma_{\mu\nu}(u)g\hat{F}_{\lambda\sigma}(v)d\sigma_{\lambda\sigma}(v)\right\rangle\right) \cong \exp(-\sigma_a S_{\min}), \tag{31}$$

$\sigma_a \sim (\mathrm{tr} gT_i gT_j) \sim C_2(a)$, where $\hat{F}_{\mu\nu} = F^{(i)}_{\mu\nu}T_i$.

In this way Eq. (31) establishes the Casimir scaling of the string tension (and gluon exchange) for any gauge group, where the Gaussian approximation holds. The latter, as shown in [43] is defined by the parameter $\sigma\lambda^2 = \sigma/M^2$, where M is the gluelump mass. In SU(3) the value of M is around $4\sqrt{\sigma}$ which establishes the $O(5\%)$ accuracy of the Casimir scaling and at same time the mass M defines the flux tube screening mass, the average value of around 1 GeV, taken above in this paper.

Now turning to another gauge group, e.g. G_2, one must calculate the gluelump masses, corresponding to one or two adjoint charges connected by confinement to the static adjoint charge, i.e. $M_0^{(1gl)}$ and $M_0^{(2gl)}$ in Eqs. (9) and (7) respectively. In this way one finds D^E and D_1^E in (1) and all flux tube distributions, like (15) are fully defined.

However, one should stress the possible differences between $\mathrm{SU}(N_c)$ and other gauge groups, e.g. G_2 or F_4. Namely, in [68] it was found, that linear confinement is screened at large R even for fundamental charges, because the string breaks into multiple adjoint charges [impossible for $\mathrm{SU}(N_c)$]. Second, in [69] the G_2 thermodynamics exhibits the large role of the diquark modes with the nearly Goldstone nature. It is clear, that this interesting field requires additional study, which can be done with the FCM formalism.

ACKNOWLEDGMENTS

The authors are grateful to P. Cea, L. Cosmai, F. Cuteri and A. Papa for providing the numerical data. This work was done in the framework of the scientific project, supported by the Russian Science Foundation Grant No. 16-12-10414.

APPENDIX: CALCULATION OF THE CORRELATOR D_1 VIA THE GLUELAMP GREEN'S FUNCTION

Consider the field correlator Eq. (1), and take into account, that $F_{\mu\nu} = \partial_\mu A_\nu - \partial_\nu A_\mu - ig[A_\mu A_\nu]$. The contribution of the first terms with derivatives immediately yields the lowest contribution in the form

$$D_1^E(x) = -\frac{2g^2}{N_c^2}\frac{dG(x)}{dx^2}, \tag{A1}$$

where $G(x)$ is the one-gluon gluelump Green's function

$$G^{(1g)}_{\mu\nu}(x,y) = \langle Tr_a A_\mu(x)\hat{\Phi}(x,y)A_\nu(y)\rangle = \delta_{\mu\nu}G(x-y) \tag{A2}$$

and $\hat{\Phi}(x,y)$ is the parallel transporter in the adjoint representation and we have exploited the Feynman gauge.

To simplify the matter we consider the gluelump Green's function as a relativistic Green's function of scalar particle with mass m (neglecting internal degrees of freedom in the first approximation), which yields

$$G(x) = \frac{(N_c^2-1)N_c}{4\pi^2}\frac{m}{|x|}K_1(m|x|), \tag{A3}$$

where K_1 is the modified Bessel function. Taking derivative in (A1), one has

$$D_1^E(x) = \frac{g^2m^2}{4\pi^2}\frac{(N_c^2-1)}{N_c}\frac{K_2(m|x|)}{x^2}. \tag{A4}$$

In the limit $m \to 0$ Eq. (A4) yields the standard one-gluon form $D_1^E(x) = \frac{16\alpha_s}{3\pi x^4}$, which generates according to (5) the color Coulomb interaction $V_1(r) = -\frac{4\alpha_s}{3r}$.

In the paper the form (A4) is used to predict the field distribution in the flux tube.

[1] M. Fukugita and T. Niuya, Phys. Lett. **132B**, 374 (1983).
[2] J. E. Kiskis and K. Sparks, Phys. Rev. D **30**, 1326 (1984).
[3] J. W. Flower and S. W. Otto, Phys. Lett. **160B**, 128 (1985).
[4] J. Wosiek and R. W. Haymaker, Phys. Rev. D **36**, 3297 (1987).
[5] A. Di Giacomo, M. Maggiore, and S. Olejnik, Phys. Lett. B **236**, 199 (1990).
[6] A. Di Giacomo, M. Maggiore, and S. Olejnik, Nucl. Phys. **B347**, 441 (1990).
[7] V. Singh, D. A. Browne, and R. W. Haymaker, Phys. Lett. B **306**, 115 (1993).
[8] P. Cea and L. Cosmai, Nucl. Phys. B, Proc. Suppl. **30**, 572 (1993).
[9] Y. Matsubara, S. Ejiri, and T. Suzuki, Nucl. Phys. B, Proc. Suppl. **34**, 176 (1994).
[10] P. Cea and L. Cosmai, Nuovo Cimento Soc. Ital. Fis. **107A**, 541 (1994).
[11] P. Cea and L. Cosmai, Nucl. Phys. B, Proc. Suppl. **34**, 219 (1994).
[12] P. Cea and L. Cosmai, Phys. Lett. B **349**, 343 (1995).
[13] P. Cea and L. Cosmai, Nucl. Phys. B, Proc. Suppl. **42**, 225 (1995).
[14] P. Cea and L. Cosmai, Phys. Rev. D **52**, 5152 (1995).
[15] G. S. Bali, K. Schilling, and C. Schlichter, Phys. Rev. D **51**, 5165 (1995).
[16] R. W. Haymaker and T. Matsuki, Phys. Rev. D **75**, 014501 (2007).
[17] A. D'Alessandro, M. D'Elia, and L. Tagliacozzo, Nucl. Phys. **B774**, 168 (2007).
[18] M. S. Cardaci, P. Cea, L. Cosmai, R. Falcone, and A. Papa, Phys. Rev. D **83**, 014502 (2011).
[19] P. Cea, L. Cosmai, and A. Papa, Phys. Rev. D **86**, 054501 (2012).
[20] P. Cea, L. Cosmai, F. Cuteri, and A. Papa, *Proc. Sci.*, LATTICE2013 (2013) 468, [arXiv:1310.8423].
[21] P. Cea, L. Cosmai, F. Cuteri, and A. Papa, Phys. Rev. D **89**, 094505 (2014).
[22] P. Cea, L. Cosmai, F. Cuteri, and A. Papa, *Proc. Sci.*, LATTICE2014 (2014) 350, [arXiv:1410.4394].
[23] N. Cardoso, M. Cardoso, and P. Bicudo, Phys. Rev. D **88**, 054504 (2013).
[24] M. Caselle, M. Panero, R. Pellegrini, and D. Vadacchino, J. High Energy Phys. 01 (2015) 105.
[25] G.'t Hooft, in *High Energy Physics, EPS International Conference, Palermo, 1975*, edited by A. Zichichi (Editrice Compositori, Bologna, 1976), https://books.google.ru/books?id=3RaJvgAACAAJ.
[26] S. Mandelstam, Phys. Rep. **23**, 245 (1976).
[27] G. Ripka, Lect. Notes Phys. **639**, 1 (2004).
[28] K.-I. Kondo, S. Kato, A. Shibata, and T. Shinohara, Phys. Rep. **579**, 1 (2015).
[29] H. G. Dosch, Phys. Lett. B **190**, 177 (1987).
[30] H. G. Dosch and Yu. A. Simonov, Phys. Lett. B **205**, 339 (1988).
[31] Yu. A. Simonov, Nucl. Phys. **B307**, 512 (1988).
[32] Yu. A. Simonov, in *QCD: Perturbative or Nonperturbative? Proc. of the XVII Autumn School, Lisbon, Portugal*, edited by S. Ferreira, P. Nogueira, and J. I. Silva-Marcos (World Scientific, Singapore, 2000), http://www.worldscientific.com/worldscibooks/10.1142/4432.
[33] A. M. Badalian, Yu. A. Simonov, and V. I. Shevchenko, Yad. Fiz. **69**, 1818 (2006) [Phys. Atom. Nucl. **69**, 1781 (2006)].
[34] Yu. A. Simonov, Int. J. Mod. Phys. A **31**, 1650016 (2016).
[35] Yu. A. Simonov, Phys. At. Nucl. **58**, 107 (1995).
[36] A. V. Nefediev, Yu. A. Simonov, and M. A. Trusov, Int. J. Mod. Phys. E **18**, 549 (2009).
[37] Yu. A. Simonov, Nucl. Phys. **B592**, 350 (2001).
[38] I. Jorysz and C. Michael, Nucl. Phys. **B302**, 448 (1988).
[39] N. Campbell, I. Jorysz, and C. Michael, Phys. Lett. **167B**, 91 (1986).
[40] Yu. A. Simonov, Phys. At. Nucl. **69**, 528 (2006).
[41] Yu. A. Simonov and V. I. Shevchenko, Adv. High Energy Phys. **2009**, 873051 (2009).
[42] Yu. A. Simonov, Proc. Steklov Inst. Math. **272**, 223 (2011).
[43] Yu. A. Simonov, Phys. Usp. **39**, 313 (1996).
[44] D. S. Kuzmenko, V. I. Shevchenko, and Yu. A. Simonov, Phys. Usp. **47**, 1 (2004).
[45] N. O. Agasian, M. S. Lukashov, and Yu. A. Simonov, Eur. Phys. J. A **53**, 138 (2017).
[46] P. Cea, L. Cosmai, F. Cuteri, and A. Papa, Phys. Rev. D **95**, 114511 (2017).
[47] P. Bicudo and V. Cardoso, Phys. Rev. D **85**, 077501 (2012).
[48] P. Bicudo, N. Cardoso, and M. Cardoso, Acta Phys. Pol. B Proc. Suppl. **9**, 447 (2016).

[49] P. Cea, L. Cosmai, F. Cuteri, and A. Papa, J. High Energy Phys. 06 (2016) 033.
[50] Yu. A. Simonov, arXiv:1605.07060.
[51] S. Gupta, K. Hübner, and O. Kaczmarek, Nucl. Phys. **A785**, 278 (2007).
[52] Yu. A. Simonov, Phys. At. Nucl. **68**, 1294 (2005).
[53] G. S. Bali, Phys. Rep. **343**, 1 (2001).
[54] T. Kawanai and S. Sasaki, Phys. Rev. Lett. **107**, 091601 (2011).
[55] K. Chung and J. Greensite, Phys. Rev. D **96**, 034512 (2017).
[56] A. Di Giacomo, E. Meggiolaro, and H. Panagopoulos, Nucl. Phys. **B483**, 371 (1997).
[57] M. D'Elia, A. Di Giacomo, and E. Meggiolaro, Phys. Rev. D **67**, 114504 (2003).
[58] A. Di Giacomo, H. G. Dosch, V. I. Shevchenko, and Yu. A. Simonov, Phys. Rep. **372**, 319 (2002).
[59] M. Baker, N. Brambilla, H. G. Dosch, and A. Vairo, Phys. Rev. D **58**, 034010 (1998).
[60] J. R. Clem and J. Low, Temp. Phys. **18**, 427 (1975).
[61] M. Baker, Phys. Rev. D **93**, 054012 (2016).
[62] V. D. Mur, V. S. Popov, Yu. A. Simonov, and V. P. Yurov, J. Exp. Theor. Phys. **78**, 1 (1994).
[63] Yu. A. Simonov, JETP Lett. **106**, 135 (2017).
[64] A. V. Nefediev and Yu. A. Simonov, Phys. Rev. D **76**, 074014 (2007).
[65] Yu. A. Simonov, Int. J. Mod. Phys. A **31**, 1650104 (2016).
[66] M. Cardoso, N. Cardoso, and P. Bicudo, Phys. Rev. D **81**, 034504 (2010).
[67] V. I. Shevchenko and Yu. A. Simonov, Phys. Rev. D **65**, 074029 (2002).
[68] B. Wellegehausen, A. Wipf, and C. Wozar, Phys. Rev. D **83**, 016001 (2011).
[69] A. Maas, L. von Smekal, B. Wellegehausen, and A. Wipf, Phys. Rev. D **86**, 111901(R) (2012).
[70] M. Bruno, M. Caselle, M. Panero, and R. Pellegrini, J. High Energy Phys. 03 (2015) 057.